Impacts of ENSO On The Seasonal Transition From Summer to Winter in East Asia

Sunyong Kim
Yonsei University
Jong-Seong Kug (jskug1@gmail.com)
POSTECH: Pohang University of Science and Technology

Research Article

Keywords: ENSO, Teleconnections, Seasonal transition, CMIP5

Posted Date: March 24th, 2021

DOI: https://doi.org/10.21203/rs.3.rs-335202/v1

Version of Record: A version of this preprint was published at Climate Dynamics on November 16th, 2021. See the published version at https://doi.org/10.1007/s00382-021-06019-w.

Abstract

The El Niño-Southern Oscillation (ENSO) has seasonally distinct impacts on the East Asian climate so that its seasonal transition depends on the phases of El Niño and La Niña. Here, we investigate the seasonal transition of surface temperature in East Asia from boreal summer to winter based on the warm/cold ENSO developing phases. During La Niña years, from summer to winter the continuous temperature drop in East Asia tends to be faster than that during El Niño, indicating a latter start and earlier termination of fall. This different seasonal transition in East Asia according to phases of ENSO is mostly explained by atmospheric responses to the seasonally-dependent tropical/subtropical precipitation forcings in ENSO developing phases. The anomalous positive precipitation in the subtropical North Pacific exists only in September and leads to the subtropical cyclonic flow during El Niño years. The resultant northerly anomalies on the left side of subtropical cyclone are favorable for transporting cold advection towards East Asia. However, the positive subtropical precipitation disappears and teleconnection to East Asia is strongly controlled by the negative precipitation anomalies in the western North Pacific, modulating the anticyclonic anomalies in East Asia during the early winter (November). Therefore, these seasonally sharp precipitation changes associated with ENSO evolution induce distinctive teleconnection changes from northerly (summer) to southerly (winter) anomalies, which eventually affect seasonal transition in East Asia. Also, the Coupled Model Intercomparison Project Phase 5 models reasonably simulate the relatively rapid temperature transition in East Asia during La Niña years, supporting the observational argument.

1. Introduction

Considerable progress has been made towards understanding the extratropical atmospheric response to the tropical forcing associated with El Niño-Southern Oscillation (ENSO) sea surface temperature (SST) anomalies (Yeh et al. 2018). The Rossby wave dynamics lead to changes in the extratropical atmospheric circulation, as a direct response to the ENSO-related tropical diabatic heating (Horel and Wallace 1981; Hoskins and Karoly 1981). Indeed, many previous studies suggested that the ENSO can influence the East Asian monsoon system in boreal summer (Nitta 1987; Huang and Wu 1989; Zhang et al. 1996; Kosaka and Nakamura 2006; Xie et al. 2009; Xie et al. 2016). The impacts of ENSO on the East Asian climate are also significant during the El Niño mature phase (i.e. winter), through the tropics-extratropics teleconnection (Rasmusson and Carpenter 1982; Zhang et al. 1999; Wang et al. 2000; Son et al. 2014; Gong et al. 2015; Kim et al. 2017; Kim and Kug 2018; Kim et al. 2018).

An observational study (Nitta 1987) hypothesized that during post-El Niño summers an anomalous anticyclone in the western North Pacific (WNP) can affect the summer climate in East Asia through atmospheric meridional dipoles, referred to as the Pacific-Japan (PJ) pattern. This lower-tropospheric teleconnection has been extensively considered as one of the common summer teleconnection patterns in East Asia (Nitta 1987; Huang 1992; Huang and Sun 1992). Zhang et al. (1996) found that the suppressed convective activity over the equatorial western Pacific, as a result of warming in the eastern Pacific, intensifies the East Asian summer monsoon. Strong positive anomalies of outgoing longwave

radiation over the Maritime Continent lead to the atmospheric cooling that accompanies the anomalous anticyclone. In a subsequent study, the intensified and westward shift of the anticyclonic anomalies in the WNP was suggested to be responsible for the negative precipitation anomalies over both southern and northern parts of China, and bounding positive anomalies over central parts (Zhang et al. 1999).

Evidence presented in Wang et al. (2000) also shows that the recurrent anomalous anticyclone after an El Niño event is a result of an atmospheric Rossby wave response to the SST cooling over the WNP. The WNP anticyclonic anomalies persist until the following summer through positive thermocline feedback between the anticyclone and negative SST anomalies. In accordance with summer, the WNP anticyclonic anomalies act as a key system that bridges the ENSO and East Asian winter monsoon, transporting warm and moist air towards East Asia (Wang et al. 2000). Previous studies on the ENSO impacts have mainly focused on the East Asian summer and winter monsoons, but the dynamical influences of ENSO are somewhat independent on the season (Zhang et al. 1999; Wang et al. 2000; Wu et al. 2003).

In addition, Wu et al. (2003) documented the spatial-temporal evolution of ENSO-related rainfall anomalies in East Asia. Because the rainband in East Asia exhibits large meridional migration over the seasons (Tao and Chen 1987), it is necessary to understand how ENSO affects anomalous rainfall changes differently with the season. According to Wu et al. (2003), the most robust influence of ENSO is seen as a positive correlation that migrates from southern China in the fall of the ENSO developing phase to eastern-central China and southern Japan through the following spring. Another is a negative correlation over northern China in summer and fall during the ENSO developing years. These two main rainfall anomalies in East Asia are induced by different anomalous atmospheric circulation systems (Wu et al. 2003). The evolution of positive rainfall in southern China is closely related to the lower-level anticyclone anomalies over the WNP. The anticyclonic anomalies are established over the South China Sea in fall of ENSO developing years, move eastward to the Philippine Sea during the ENSO mature phase, and shift northward in spring and summer of ENSO decaying years. In comparison, the negative rainfall in northern China is associated with the northerly anomalies on the western side of the cyclonic anomalies that displace southwestward along the East Asian coast during the developing phase of ENSO.

More recently, Son et al. (2016) suggested that a significant negative correlation exists in September, the ENSO developing phase, between Niño3 SST and precipitation over the Korean Peninsula. Interestingly, the positive precipitation anomalies that exist over the subtropical North Pacific associated with ENSO can be considered a unique pattern only in this month. This subtropical diabatic heating in September plays a critical role in generating the cyclonic flow over the subtropical North Pacific as a Rossby wave response. The resultant northerly anomalies on the left side of cyclonic circulation act to decrease the precipitation over the Korean Peninsula in September. Therefore, Son et al. (2016) emphasized that the subtropical cyclone is a key component in linking ENSO signals to East Asia accompanying the northerly anomalies in September.

Despite the above studies on the seasonally-varying ENSO teleconnections in East Asia, detailed studies focusing on the ENSO-related seasonal transition have not been conducted sufficiently. In particular, the ENSO possibly contributes to the seasonal transition from summer to winter; owing to the East Asian perturbations associated with ENSO being considerably different in summer and winter, respectively. Although limited studies have investigated this season, there still remains a need to understand the ENSO impacts on the East Asian fall climate in terms of its spatial/temporal evolution, intensity, and dynamical processes. Therefore, in this study, we investigate the ENSO impacts on seasonal transition, in particular from summer to winter (i.e., fall) in East Asia.

The fall, namely autumn, can be defined diversely but simply refers to the season between summer and winter. Astronomically, fall is regarded in the Northern Hemisphere as from the fall equinox to the winter solstice. In meteorology, fall is generally considered to include the months of September, October, and November in the Northern Hemisphere; March, April, and May in the Southern Hemisphere. We compare the atmospheric seasonal transition and its regional impacts on East Asia, from summer to winter, related to the ENSO forcings using observational data. In addition, we assess how well the Coupled Model Intercomparison Project Phase 5 (CMIP5) models simulate the ENSO impacts on seasonal transition during fall in East Asia.

Section 2 describes the observed and simulated datasets. Section 3 examines the ENSO-related seasonal transition in East Asia with the observed results. In Sect. 4, the long-term climate simulations of CMIP5 models are investigated to support the observational findings, and the fidelity of seasonal transition in current models is also evaluated. A summary and discussion follow in Sect. 5.

2. Data

2.1 Reanalysis and Observation data

Observations used in this study are from a total of 400 weather stations in China, Korea, and Japan. The monthly surface temperature and precipitation data include 160 stations in China (China Meteorological Administration; CMA), 87 stations in Korea (Korea Meteorological Administration, KMA), and 153 stations in Japan (Japan Meteorological Agency, JMA). The daily mean temperature and precipitation data only available at 45 stations over South Korea from KMA are also used. The monthly SST data are derived from the Extended Reconstructed Sea Surface Temperature version 5 (ERSSTv5; Huang et al. (2017)). The daily and monthly atmospheric variables are obtained using the NCEP-DOE AMIP-II Reanalysis (R-2) from the National Centers for Environmental Prediction/National Center for Atmospheric Research (NCEP/NCAR; Kanamitsu et al. (2002)). Monthly precipitation data are also obtained from the Climate Prediction Center Merged Analysis of Precipitation (CMAP; Xie and Arkin (1997)). The hourly precipitation data of the European Centre for Medium-range Weather Forecasts (ECMWF; Hersbach et al. (2020)) fifth generation reanalysis (ERA5) are utilized on a daily scale. All reanalysis data cover the period from 1979 to 2018. Note the seasonal cycle and linear trend are removed from the data before analysis.

2.2 CMIP5 models

Historical simulations produced by the 40 Coupled Model Intercomparison Project Phase 5 (CMIP5) models were analyzed. A single ensemble member (r1i1p1, the first realization of the first initialization of the perturbed physics model) of each model is used in this study. Brief descriptions of the 40 models including their modeling centers are listed in Table 1. An overview of CMIP5 and the experiment design are described by Taylor et al. (2012). We utilized the monthly-mean outputs for a total of 100-year integrations from 1901 to 2000. Data of all CMIP5 models were also linearly detrended.

Table 1
List of the models from the CMIP5 archive used in this study and their respective institutes.

Model	Institute, Country
bcc-csm1-1	BCC, CMA, China
bcc-csm1-1-m	BCC, CMA, China
BNU-ESM	GCESS, China
CanESM2	CCCMA, Canada
CESM1-BGC	NSF-DOE-NCAR, USA
CESM1-CAM5	NSF-DOE-NCAR, USA
CESM1-FASTCHEM	NSF-DOE-NCAR, USA
CESM1-WACCM	NSF-DOE-NCAR, USA
CMCC-CESM	CMCC, Italy
CMCC-CM	CMCC, Italy
CMCC-CMS	CMCC, Italy
CNRM-CM5	CNRM-CERFACS, France
CSIRO-Mk3-6-0	CSIRO-QCCCE, Australia
FGOALS-g2	LASG-CESS, China
FIO-ESM	FIO, SOA, China
GFDL-CM3	NOAA-GFDL, USA
GFDL-ESM2G	NOAA-GFDL, USA
GFDL-ESM2M	NOAA-GFDL, USA
GISS-E2-H	NASA/GISS, USA
GISS-E2-H-CC	NASA/GISS, USA
GISS-E2-R	NASA/GISS, USA
GISS-E2-R-CC	NASA/GISS, USA
HadCM3	MOHC, UK
HadGEM2-AO	NIMR-KMA, Korea/UK
HadGEM2-CC	MOHC, UK
HadGEM2-ES	MOHC, UK

Model	Institute, Country
inmcm4	INM, Russia
IPSL-CM5A-LR	IPSL, France
IPSL-CM5A-MR	IPSL, France
IPSL-CM5B-LR	IPSL, France
MIROC5	AORI-NIES-JAMSTEC, Japan
MIROC-ESM	AORI-NIES-JAMSTEC, Japan
MIROC-ESM-CHEM	AORI-NIES-JAMSTEC, Japan
MPI-ESM-LR	MPI-M, Germany
MPI-ESM-MR	MPI-M, Germany
MPI-ESM-P	MPI-M, Germany
MRI-CGCM3	MRI, Japan
MRI-ESM1	MIR, Japan
NorESM1-M	NCC, Norway
NorESM1-ME	NCC, Norway

3. Seasonal Transition In East Asia Related To Enso

3.1 Relationship between ENSO and seasonal transition in East Asia

Figure 1 shows composites of the daily surface temperature and precipitation over South Korea from summer to winter (August-December) for the developing phases of El Niño and La Niña. The El Niño (La Niña) years are defined when the fall season (September-November; SON) Niño3.4 (170°E-120°W, 5°S-5°N) SST exceeds its 0.5 (-0.5) standard deviation, resulting in a total of 12 (13) years. The temperature and precipitation data over South Korea are smoothed by the 11-day moving average to remove short-term fluctuations. The temperature over South Korea gradually decreases from summer to winter for both El Niño and La Niña years, showing the evident seasonal transition. However, the decreasing trend appears to be stronger in La Niña years compared to that of El Niño years (Fig. 1a). Figure 1b shows the temperature difference between El Niño and La Niña events over South Korea. It shows that the South Korean temperature is higher in La Niña than in El Niño years from late summer to mid-fall (August and October), but the opposite is found from early-November onwards. Such temperature differences between El Niño and La Niña years over South Korea are mostly significant at the 95% confidence level based on bootstrap analysis with 10,000 times random sampling.

Over South Korea, heavy rainfall is predominantly experienced during summer, rapidly decreasing before winter, in both El Niño and La Niña years (Fig. 1c). The precipitation difference between El Niño and La Niña years shows that South Korean precipitation is higher in La Niña than in El Niño years until mid-October (Fig. 1d), almost consistent with temperature transition. According to Fig. 1, the surface temperature and precipitation over South Korea tend to be higher in La Niña than in El Niño years until October but reverses after October. Therefore, during the ENSO developing phase, the detailed temporal evolution of the ENSO warm and cold years is somewhat different over South Korea.

These temperature and precipitation differences in the El Niño and La Niña evolutions may affect the period of fall. Here, the fall period is defined as the mean daily temperature between the last sequence day above 5℃ and the first sequence day below 20℃ (Table 2) following Lee (1979). Averaged over 40 years, fall over South Korea totals 69 days, from 19th September to 26th November. During El Niño years, the number of days classified as fall over South Korea is 75. However, during La Niña, fall starts 5 days later and terminates 6 days earlier. Therefore, the period of South Korean fall for La Niña is 11 days shorter than that for El Niño years. This means that the seasonal transition in surface temperature from summer to winter over South Korea tends to be much faster during La Niña than that of El Niño years. Note that these results are robust to the temperature criteria used for the definition of the fall period.

Table 2
The fall period and number of days at 45 weather stations over South Korea for El Niño, normal and La Niña years, based on the ±0.5 standard deviation of SON Niño3.4 (170°-120°W, 5°S-5°N) SST. The fall period is defined as the mean daily temperature between the last sequence day above 5℃ and the first sequence day below 20℃ as in Lee (1979).

Type	Period	Days
El Niño	16 September ~ 29 November	75 days
Normal	19 September ~ 26 November	69 days
La Niña	21 September ~ 23 November	64 days

To assess whether the result over South Korea extends over a wider region, the same analysis as in Fig. 1 is also applied for surface temperature particularly over the Korea-Japan region (120°E-145°E, 30°N-40°N) using the reanalysis data (Fig. 2). Overall, temperature trends for Korea-Japan are similar to those of South Korea (Fig. 1a) with gradual decreases in temperature for both El Niño and La Niña years (Fig. 2a). The temperature difference between El Niño and La Niña years is also consistent with the station results over South Korea (Fig. 1b), indicating that temperature is higher in La Niña than in El Niño years until early-November and then the opposite occurs afterward (Fig. 2b). Similarly, Korea and Japan experience distinctly more rainfall in La Niña than El Niño until late-October, but the opposite pattern occurs from November (Fig. 2d). Overall, the East Asian climate rapidly changes during La Niña years from summer to winter, showing a steeper slope than those during El Niño.

To examine the seasonal transition in East Asia during the ENSO developing phase, Fig. 3 shows the regressed temperature and precipitation in East Asia with respect to SON Niño3.4 SST using data from 400 weather stations throughout China, Korea, and Japan. In September, there are negative temperature anomalies overall at most stations (Fig. 3a). In particular, the negative temperature anomalies are significant over the lower reaches of the Yangtze River in China, Korea, and Japan. In November, the negative temperature anomalies exist over China but are insignificant at most stations, except for a few stations around Shandong (Fig. 3b). Interestingly, positive temperature anomalies are dominant over Korea and Japan in November implying that the East Asian temperature responses to El Niño forcing are different between September and November. In comparison, the temperature difference between September and November shows the evident positive anomalies over the southern coast of China, Korea, and Japan (Fig. 3c). It is noted that the overall correlation with the temperature difference is much higher than those within each month (not shown). The regressed precipitation anomalies in September are similar to the temperature pattern, but significant anomalies are mostly confined over Korea (Fig. 3d). In November, significant positive correlations exist at most weather stations throughout southeastern China, Korea, and Japan (Fig. 3e). Consistent with the temperature difference (Fig. 3c), the precipitation difference between September and November in East Asia shows the overall positive anomalies, again higher than those of each month's precipitation (Fig. 3f).

The temperature difference between September and November with respect to SON Niño3.4 SST shows positive anomalies dominant over Korea and Japan (Fig. 3c). Simply, the temperature anomalies in East Asia have a negative tendency from September to November as shown in Figs. 1a and 2a. Therefore, the positive anomalies found in their difference indicate that the seasonal temperature tendency slows down as the El Niño increases, while the temperature decreases steeply from summer to winter when La Niña intensifies in amplitude. The seasonal precipitation tendency from September to November overall also shows positive anomalies in East Asia indicating the dramatic precipitation change during the La Niña evolution (Fig. 3f), as exhibited in Figs. 1c and 2c. Therefore, a key question remains as to the transition speeds, and why the impacts of El Niño and La Niña forcing on the East Asian climate are seasonally different. During the ENSO developing phase, the temperature/precipitation tendencies in East Asia can be explained by the ENSO-related tropical forcing and resultant atmospheric circulation. The detailed underlying dynamical processes, that are associated with the different seasonal transitions in East Asia will be examined in the next section.

3.2 Seasonal ENSO teleconnections to East Asia

To investigate the seasonal transition responses to ENSO in East Asia, the regressed precipitation and lower-tropospheric circulation with respect to SON Niño3.4 SST are calculated (Fig. 4). In September, the typical ENSO-related precipitation pattern over the tropical Pacific is characterized by a dipole with negative precipitation anomalies in the western Pacific and zonally-extended positives from the equatorial central to eastern Pacific (Fig. 4a). The positive precipitation anomalies centered over the equatorial central Pacific (CP) induce a lower-level cyclonic flow in both hemispheres as a Gill-type response, but its meridional extent is confined in the off-equatorial and some subtropical regions.

Interestingly, the distinct positive precipitation anomalies appear over the subtropical North Pacific around 10°N, which is a unique pattern only in this season (Son et al. 2016). The subtropical positive precipitation anomalies likely play a role in extending the subtropical cyclonic anomalies further northward by causing additional subtropical diabatic heating (Son et al. 2016). The resultant cyclonic anomalies are dominant over the subtropical North Pacific, accompanied by northerly wind anomalies on the western side of cyclonic circulation (Fig. 4d). The low-level northerly wind anomalies near the south of Korea are favorable for cold air and dry advection over the Korea-Japan region in September (Fig. 3a, d).

In November, the teleconnection pattern in East Asia is quite different from that in September. In addition, the distinct positive precipitation anomalies, which occur over the subtropical North Pacific in September, clearly disappear in November, and the overall negative anomalies in the WNP are dominant (Fig. 4b). The negative WNP precipitation anomalies are responsible for the strong anticyclonic anomalies near East Asia conveying the southerly anomalies on the western side of the circulation ((Son et al. 2014; Kim et al. 2017; Kim and Kug 2018; Kim et al. 2018). The lower-tropospheric anticyclonic anomalies in the WNP are vertically baroclinic, therefore are accompanied by cyclonic anomalies in the upper troposphere. The upper-tropospheric divergence related to the cyclonic circulation drives the anticyclonic anomalies near East Asia through Rossby wave energy propagation (Fig. 4e). Therefore, in November the WNP precipitation anomalies can modulate temperature and precipitation variability in East Asia.

The precipitation difference between September and November shows negative in the WNP and positive in the equatorial CP (Fig. 4c). The WNP (110°E-150°E, 0°-15°N) and equatorial CP (160E°-120°W, 5°S-5°N) precipitation anomalies in November are 1.46 and 1.42 times stronger than those in September, respectively. For the ENSO-related seasonal difference in atmospheric circulation, anticyclonic anomalies in East Asia accompany the southerly anomalies (Fig. 4f). The anticyclonic anomalies near East Asia in the circulation differences between September and November are directly linked to the temperature and precipitation results evident at weather stations in Fig. 3c, f. Based on the circulation patterns in September and November, the meridional wind directions show a tendency, from northerly to southerly anomalies, over East Asia (Fig. 4d, e). From September to November, the southerly tendency in East Asia occurs slower during El Niño, and faster during La Niña. These results clearly demonstrate that the seasonal transition of atmospheric circulation over East Asia, from summer to winter, is relatively rapid during the La Niña years. Therefore, in East Asia, the atmospheric tendency of ENSO developing warm and cold phases is mostly explained by the dynamical atmospheric responses to the different tropical/subtropical precipitation forcings in September and November, respectively.

4. Cmip5 Model Simulation

4.1 Simulation of seasonal transition in East Asia

In the previous section, the observed seasonal transition in the East Asian climate associated with the ENSO developing phase was examined and the leading role of tropical/subtropical diabatic forcing was suggested. Here, the same analysis as in Fig. 4 using CMIP5 simulations is repeated to further

understand the ENSO-related seasonal transition in East Asia (Fig. 5). The CMIP5 models simulate the observed precipitation pattern reasonably well, exhibiting the negative anomalies in the western Pacific and zonally-extended positive anomalies spanning the equatorial CP to eastern Pacific in September and November (Fig. 5a, b). Although the CMIP5 models represent well the dominant observed features, the ENSO-induced precipitation centers in the tropics tend to be shifted westward (Ham and Kug 2015). In addition, the CMIP5 models also underestimate the magnitude of regressed precipitation anomalies related to the El Niño forcing (Kim et al. (2017).

In September, the negative precipitation anomalies are confined south of the equator, while the equatorial CP and subtropical positive precipitation anomalies exist (Fig. 5a) though they are weaker than the observed (Fig. 4a). The weaker subtropical precipitation anomalies lead to weaker cyclonic circulation anomalies over the subtropical North Pacific, and their center locates further northeastward (Fig. 5d) compared to the observations (Fig. 4d). The resultant northerly wind anomalies on the western side of cyclonic circulation are also weaker but remain significant near East Asia. In November the CMIP5 models tend to simulate well the negative precipitation anomalies in the WNP and positives in the equatorial CP, although they underestimate the magnitude (Fig. 5b) compared to the observed pattern (Fig. 4b). As a result, the anticyclonic anomalies are similarly weaker and confined in the subtropics south of 40°N (Fig. 5e) than the observed (Fig. 4e). It is also shown here that the subtropical positive precipitation anomalies, the dominant feature of September, diminish during November in the case of the CMIP5 model pattern.

From the ENSO-related precipitation difference between September and November, the CMIP5 models reproduce well the strengthening of positive precipitation anomalies in the equatorial CP (Fig. 5c). In the WNP region, the negative precipitation anomalies also intensify between September and November, consistent with the observations (Fig. 4c). Therefore, the atmospheric differences between September and November show the anticyclonic anomalies near East Asia accompanying the southerlies on the western side of circulation (Fig. 5f). These results suggest that the CMIP5 models have an ability in reproducing the observed rapid transition in East Asia during the La Niña years, although the simulated magnitudes are relatively weaker than those of the observed.

4.2 Intermodel diversity of seasonal transition in East Asia

To examine the individual CMIP5 model performance in simulating the seasonal transition in East Asia, Fig. 6 shows the regressed air temperature tendency over the Korea-Japan region between September and November associated with ENSO for each model. The positive regression value in the temperature tendency between September and November indicates that the Korea-Japan region experiences a rapid seasonal transition during La Niña years found in Fig. 3f, 4f. The CMIP5 multimodel ensemble mean (MME) reproduces the positive temperature tendency over the Korea-Japan region but underestimates the observational magnitude accounting for only 21%. The seasonal transitions over the Korea-Japan region from September to November among the 40 individual models are diverse. Interestingly, most models simulate the positive magnitude apart from only 6 models, but no individual models exceed the observed strength.

The 40 CMIP5 models simulate diverse ENSO-related seasonal transitions in East Asia (Fig. 6) owing to a large diversity in the simulated tropical precipitation responses to the ENSO forcing among the CMIP5 models (Kim et al. 2017). To examine what determines the speed of seasonal transition in East Asia associated with ENSO, we classified the models into two groups, 10 good models with the fast seasonal transition in La Niña years (e.g., similar to the observed), and 10 poor models, based on the magnitude of seasonal transition over the Korea-Japan region as shown in Fig. 6. Note that the poor models include the 6 models which reproduce the negative transition sign opposite to the observed result.

Figures 7 and 8 display the multi-model composites of the regressed atmospheric teleconnection and precipitation pattern, respectively, with Niño3.4 SST for both the good and poor model cases. In the good models, the dominant cyclonic anomalies over the North Pacific induce the northerly wind anomalies near East Asia during September (Fig. 7a), although the center of anomalous cyclonic circulation locates more northeastward than observed (Fig. 4b). The regressed precipitation anomalies for the good models show that the positive precipitation anomalies excessively extend to the western Pacific (Fig. 8a). Thus the observed negative precipitation anomalies in the western Pacific are no longer evident in the good models. The distinct positive precipitation anomalies specifically located in the subtropical North Pacific are weak but not significant among the good models. In November, anticyclonic anomalies in East Asia accompany the southerly anomalies on the western side of the circulation feature (Fig. 7b), suggesting the possible role of the negative WNP precipitation anomalies. The negative precipitation anomalies are shown to be dominant in the WNP for the good models in November (Fig. 8b).

The atmospheric circulation tendency between September and November during the El Niño developing phase demonstrates that the anomalous southerly wind is associated with the strong anticyclonic anomalies in East Asia (Fig. 7c), consistent with the observed pattern (Fig. 4f). In the precipitation difference between September and November, the negative difference in the WNP is clearly evident (Fig. 8c). It is conceived that for the good models the seasonal transition pattern in the WNP is most realistic (Fig. 4c). Therefore, the strong anticyclonic tendency with the southerly anomalies in East Asia between September and November is presumably a response to the strengthening of negative precipitation anomalies in the WNP. These results suggest that the good models simulated well the observed rapid seasonal transition of atmospheric circulation in East Asia during the La Niña developing phases due to the realistic evolution of tropical precipitation anomalies.

Conversely, the poor models simulate the cyclonic anomalies over the North Pacific north of 40°N in September (Fig. 7d). The cyclonic anomalies induce significant westerly wind anomalies on the southwestern side of circulation in East Asia, quite different from the observed teleconnection pattern (Fig. 4d). The poor models simulate the WNP precipitation anomalies close to zero, and the observed positive precipitation anomalies in the subtropical North Pacific are not clearly captured (Fig. 8d). In November, the anticyclone anomalies are confined south of 30°N (Fig. 7e), therefore difficult to have an influence on the East Asian climate. In the atmospheric circulation tendency between September and November, the poor models simulate insignificant atmospheric circulation in East Asia (Fig. 7f). The ENSO-related negative precipitation anomalies in the WNP become stronger from September to

November (Fig. 8f), but their magnitude in their difference is weaker than in the good models (Fig. 8c). As a result, the poor models do not simulate sufficient seasonal transition of atmospheric circulation in East Asia during September and November. Therefore, the good models have better performance in the seasonal transition of atmospheric teleconnection in East Asia associated with ENSO compared to the poor models.

The results using CMIP5 models have important implications for the model fidelity of ENSO teleconnection in East Asia. In particular, the good models simulate patterns that resemble more the observed tropical/subtropical precipitation anomalies which play a dominant role in linking ENSO to the East Asian climate system. A reasonable inference is that the good models reproduce well the observed seasonal transition from boreal summer to winter in East Asia, further supporting the importance of diabatic forcing in the tropical and subtropical North Pacific.

5. Summary And Discussion

The seasonal transitions of East Asian climate during the ENSO developing warm and cold phases are investigated using observations and CMIP5 models. It is clearly shown that during the La Niña years, East Asia experiences a rapid seasonal transition from summer to winter, with a later start and earlier termination of fall, than those during El Niño years. Further, the evident difference in fall duration between El Niño and La Niña years can be dynamically explained by the seasonally different ENSO teleconnection. In September, East Asia experiences northerly wind anomalies that transport cold and dry advection as a direct response to the distinct El Niño-related positive precipitation anomalies in the subtropical North Pacific only in this month. Conversely, in November the WNP precipitation forcing is critical in developing the anticyclonic anomalies in East Asia with anomalous southerly winds associated with El Niño. In the El Niño-related seasonal transition for atmospheric circulation from September to November, the southerly anomalies in East Asia indicate that the northerly tendency (i.e., the seasonal transition of the background state) slows down during El Niño years; that is, the tendency increases during La Niña years.

The CMIP5 models simulate well the overall observed tropical/subtropical precipitation and atmospheric teleconnection patterns associated with ENSO in September and November, respectively. However, it is evident that the CMIP5 models tend to underestimate the atmospheric circulation in East Asia because the simulated tropical/subtropical precipitation anomalies are on average somewhat weaker and shifted westward than observed. In addition, the seasonal transition in East Asia is rather diverse from model to model, indicating that the transition magnitudes of the CMIP5 models are mostly weaker than observed. The performance of CMIP5 models in simulating the seasonal transition in East Asia is still limited, but some models (i.e. here the good model cases) tend to simulate more realistic tropical precipitation and atmospheric responses to ENSO forcing, supporting the observational findings.

However, most CMIP5 models have problems in simulating the observed precipitation anomalies located in the subtropical North Pacific associated with ENSO that are distinct only in September. In a comparison of the model simulations with the observed, there are several systematic errors in simulating

the ENSO-related tropical/subtropical precipitation. The CMIP5 models tend to have a stronger Intertropical Convergence Zone (ITCZ) in the central and eastern part of off-equatorial regions and weaker along the equatorial regions, than the observed in September (not shown). This pattern results from the well-known biases in the coupled models, referred to as the double ITCZ and cold tongue biases (Wittenberg et al. 2006). Although the CMIP5 models overestimate the climatological precipitation in the subtropics during September, the simulated precipitation responses to the El Niño forcing in the subtropical North Pacific are not evident. One may suggest that the precipitation variability in the subtropical North Pacific (150°E-160°W, 5°N-20°N) is not closely related to the El Niño itself, given the correlation coefficient with Niño3.4 SST in September is only 0.20. However, the correlation with the observed indices for the 40-year period examined is much higher (i.e., 0.54) than that of the CMIP5 MME. As the El Niño-induced precipitation anomalies in September are mostly confined in the equatorial Pacific, it is meaningful to have a better understanding of the relationships between tropical ENSO SST and subtropical precipitation biases in model simulations.

In this study, we conclude the linkage of tropical/subtropical precipitation and atmospheric teleconnection associated with ENSO is important for understanding the seasonal transition in East Asia. However, a question still arises of why the teleconnection responses in East Asia to El Niño and La Niña years are slightly different? Recently, Luo and Lau (2020) suggested that northeast Asia experiences more (less) frequent summer extreme heat weather during the La Niña (El Niño) developing phases as a result of the circumglobal teleconnection (CGT) pattern associated with ENSO. According to Hardiman et al. (2018), the response of southeastern China summer rainfall to El Niño/La Niña is found to be asymmetric, with no significant response following La Niña years. Therefore, it is likely that the East Asian climate does not respond to the El Niño and La Niña forcing linearly. Although the different transition speeds of fall in East Asia associated with El Niño and La Niña developing phases are the focus of the current study, the detailed spatial pattern and intensity of tropical/subtropical diabatic forcing between El Niño and La Niña, and its impact on East Asia, will be pursued in further study.

6. Declarations (Not Applicable)

6.1 Funding

This study is supported by the National Research Foundation of Korea (NRF-2018RA5A1024958).

6.2 Conflicts of interest/Competing interests

The authors have no potential conflicts of interest or competing interests to declare.

6.3 Availability of data and material

The data from weather stations are provided by the CMA (https://data.cma.cn/), KMA (http://www.kma.go.kr/), and JMA (http://www.jma.go.jp/). The ERSSTv5 (https://psl.noaa.gov/data/gridded/data.noaa.ersst.v5.html), the CMAP

(https://psl.noaa.gov/data/gridded/data.cmap.html), and the NCEP-DOE Reanalysis 2 (https://psl.noaa.gov/data/gridded/data.ncep.reanalysis2.html) data are downloaded from their website. The CMIP5 data used are available at http://cmip-pcmdi.llnl.gov/cmip5/.

6.4 Code availability

The codes for this study are available from the SK, upon reasonable request.

References

1. Gong H, Wang L, Chen W, Nath D, Huang G, Tao W (2015) Diverse influences of ENSO on the East Asian–western Pacific winter climate tied to different ENSO properties in CMIP5 models. J Clim 28:2187–2202. https://doi.org/10.1175/JCLI-D-14-00405.1
2. Ham YG, Kug JS (2015) ENSO amplitude changes due to greenhouse warming in CMIP5: Role of mean tropical precipitation in the twentieth century. Geophys Res Lett 43::422–430. https://doi.org/10.1002/2015GL066864
3. Hardiman SC, Dunstone NJ, Scaife AA, Bett PE, Li C, Lu B, Ren H-L, Smith DM, Stephan CC (2018) The asymmetric response of Yangtze river basin summer rainfall to El Niño/La Niña. Environmental Research Letters 13:024015. https://doi.org/10.1088/1748-9326/aaa172
4. Hersbach H, Bell B, Berrisford P, Hirahara S, Horányi A, Muñoz-Sabater J, Nicolas J, Peubey C, Radu R, Schepers D (2020) The ERA5 global reanalysis. Q J R Meteorol Soc 146::1999–2049. https://doi.org/10.1002/qj.3803
5. Horel JD, Wallace JM (1981) Planetary-scale atmospheric phenomena associated with the Southern Oscillation. Monthly Weather Review 109: 813–829 https://doi.org/10.1175/1520-0493(1981)109<0813:PSAPAW>2.0.CO;2.
6. Hoskins BJ, Karoly DJ (1981) The steady linear response of a spherical atmosphere to thermal and orographic forcing. Journal of the Atmospheric Sciences 38: 1179–1196 https://doi.org/10.1175/1520-0469(1981)038<1179:TSLROA>2.0.CO;2.
7. Huang B, Thorne PW, Banzon VF, Boyer T, Chepurin G, Lawrimore JH, Menne MJ, Smith TM, Vose RS, Zhang H-M (2017) Extended reconstructed sea surface temperature, version 5 (ERSSTv5): upgrades, validations, and intercomparisons. J Clim 30:8179–8205. https://doi.org/10.1175/JCLI-D-16-0836.1
8. Huang R (1992) The East Asia/Pacific pattern teleconnection of summer circulation and climate anomaly in East Asia. Journal of Meteorological Research 6:25–37
9. Huang R, Sun F (1992) Impacts of the tropical western Pacific on the East Asian summer monsoon. J Meteorol Soc Jpn 70:243–256. https://doi.org/10.2151/jmsj1965.70.1B_243
10. Huang R, Wu Y (1989) The influence of ENSO on the summer climate change in China and its mechanism. Adv Atmos Sci 6:21–32. https://doi.org/10.1007/BF02656915
11. Kanamitsu M, Ebisuzaki W, Woollen J, Yang S-K, Hnilo J, Fiorino M, Potter G (2002) NCEP–DOE AMIP-II Reanalysis (R-2). Bull Am Meteor Soc 83:1631–1644. https://doi.org/10.1175/BAMS-83-11-

1631

12. Kim S, Kug JS (2018) What controls ENSO teleconnection to East Asia? Role of western North Pacific precipitation in ENSO teleconnection to East Asia. Journal of Geophysical Research: Atmospheres 123: 10,406–410,422 https://doi.org/10.1029/2018JD028935
13. Kim S, Son H-Y, Kug J-S (2017) How well do climate models simulate atmospheric teleconnctions over the North Pacific and East Asia associated with ENSO? Clim Dyn 48:971–985. https://doi.org/10.1007/s00382-016-3121-8
14. Kim S, Son H-Y, Kug J-S (2018) Relative roles of equatorial central Pacific and western North Pacific precipitation anomalies in ENSO teleconnection over the North Pacific. Clim Dyn 51:4345–4355. https://doi.org/10.1007/s00382-017-3779-6
15. Kosaka Y, Nakamura H (2006) Structure and dynamics of the summertime Pacific–Japan teleconnection pattern. Q J R Meteorol Soc 132::2009–2030. https://doi.org/10.1256/qj.05.204
16. Lee B-s (1979) A study of natural seasons in Korea. Journal of the Korean Geographical Society 20::1–11
17. Luo M, Lau N-C (2020) Summer heat extremes in northern continents linked to developing ENSO events. Environmental Research Letters 15:074042. https://doi.org/10.1088/1748-9326/ab7d07
18. Nitta T (1987) Convective activities in the tropical western Pacific and their impact on the Northern Hemisphere summer circulation. J Meteorol Soc Jpn 65:373–390. https://doi.org/10.2151/jmsj1965.65.3_373
19. Rasmusson EM, Carpenter TH (1982) Variations in tropical sea surface temperature and surface wind fields associated with the Southern Oscillation/El Niño. Monthly Weather Review 110: 354–384 https://doi.org/10.1175/1520-0493(1982)110<0354:VITSST>2.0.CO;2.
20. Son H-Y, Park J-Y, Kug J-S (2016) Precipitation variability in September over the Korean Peninsula during ENSO developing phase. Clim Dyn 46:3419–3430. https://doi.org/10.1007/s00382-015-2776-x
21. Son H-Y, Park J-Y, Kug J-S, Yoo J, Kim C-H (2014) Winter precipitation variability over Korean Peninsula associated with ENSO. Clim Dyn 42:3171–3186. https://doi.org/10.1007/s00382-013-2008-1
22. Tao SY, Chen L (1987) A review of recent research on the East Asian summer monsoon in China. Monsoon meteorology: 60–92
23. Taylor KE, Stouffer RJ, Meehl GA (2012) An overview of CMIP5 and the experiment design. Bulletin of the American meteorological Society 93:485–498. https://doi.org/10.1175/BAMS-D-11-00094.1
24. Wang B, Wu R, Fu X (2000) Pacific–East Asian teleconnection: how does ENSO affect East Asian climate? Journal of Climate 13: 1517–1536 https://doi.org/10.1175/1520-0442(2000)013<1517:PEATHD>2.0.CO;2.
25. Wittenberg AT, Rosati A, Lau N-C, Ploshay J (2006) GFDL's CM2 global coupled climate models. Part III: Tropical Pacific climate and ENSO. J Clim 19:698–722. https://doi.org/10.1175/JCLI3631.1

26. Wu R, Hu Z-Z, Kirtman BP (2003) Evolution of ENSO-related rainfall anomalies in East Asia. Journal of Climate 16: 3742–3758 https://doi.org/10.1175/1520-0442(2003)016<3742:EOERAI>2.0.CO;2.
27. Xie P, Arkin PA (1997) Global precipitation: A 17-year monthly analysis based on gauge observations, satellite estimates, and numerical model outputs. Bulletin of the American Meteorological Society 78: 2539–2558 https://doi.org/10.1175/1520-0477(1997)078<2539:GPAYMA>2.0.CO;2.
28. Xie S-P, Hu K, Hafner J, Tokinaga H, Du Y, Huang G, Sampe T (2009) Indian Ocean capacitor effect on Indo–western Pacific climate during the summer following El Niño. J Clim 22:730–747. https://doi.org/10.1175/2008JCLI2544.1
29. Xie S-P, Kosaka Y, Du Y, Hu K, Chowdary JS, Huang G (2016) Indo-western Pacific ocean capacitor and coherent climate anomalies in post-ENSO summer: A review. Adv Atmos Sci 33:411–432. https://doi.org/10.1007/s00376-015-5192-6
30. Yeh SW, Cai W, Min SK, McPhaden MJ, Dommenget D, Dewitte B, Collins M, Ashok K, An SI, Yim BY (2018) ENSO atmospheric teleconnections and their response to greenhouse gas forcing. Rev Geophys 56:185–206. https://doi.org/10.1002/2017RG000568
31. Zhang R, Sumi A, Kimoto M (1996) Impact of El Niño on the east Asian monsoon. J Meteorol Soc Jpn 74:49–62. https://doi.org/10.2151/jmsj1965.74.1_49
32. Zhang R, Sumi A, Kimoto M (1999) A diagnostic study of the impact of El Niño on the precipitation in China. Adv Atmos Sci 16:229–241. https://doi.org/10.1007/BF02973084

Figures

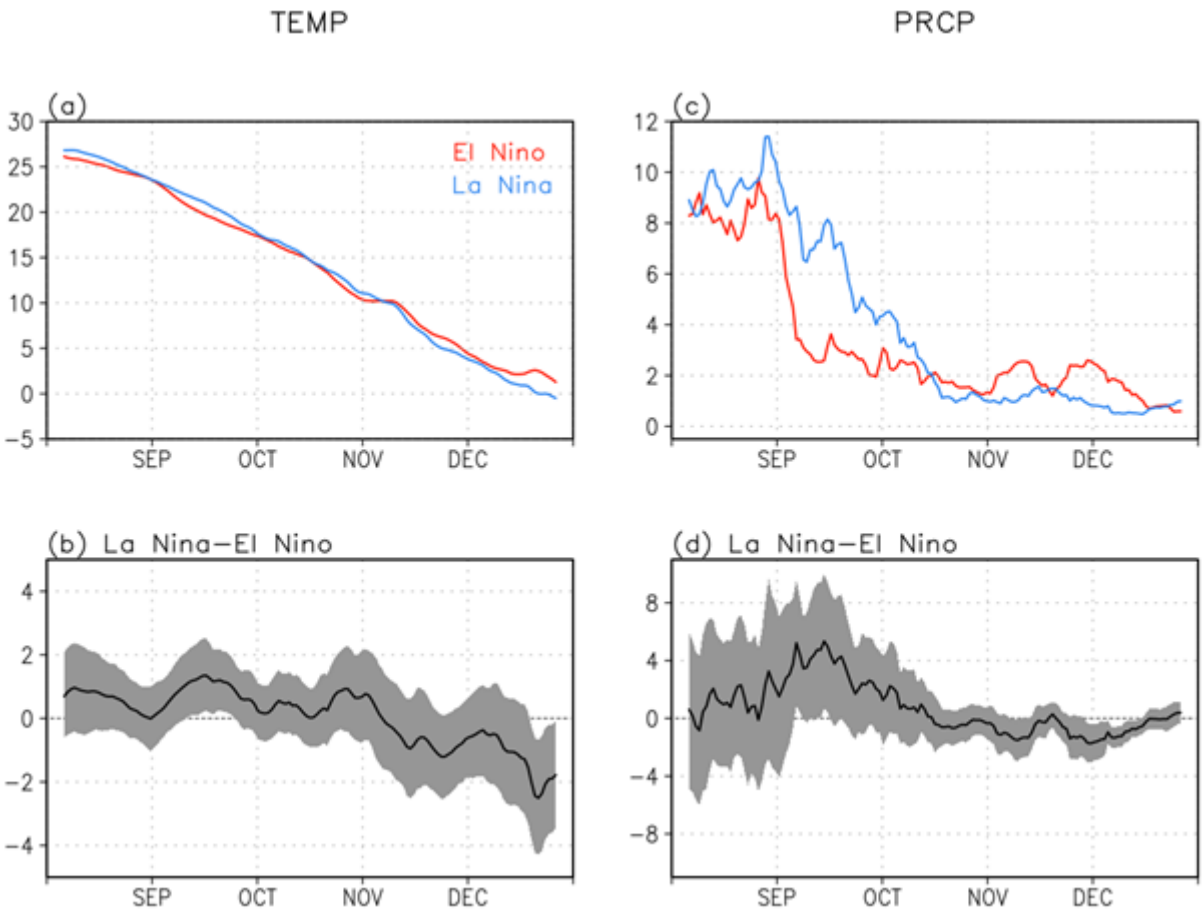

Figure 1

Mean daily (a) temperature and (c) precipitation from August to December at 45 weather stations over South Korea for the El Niño (red line; °C) and La Niña (blue line; mm/day) years based on the ±0.5 standard deviation of SON Niño3.4 (170°-120°W, 5°S-5°N) SST. Difference in the (b) temperature and (d) precipitation between El Niño and La Niña years. Temperature and precipitation data are filtered with an 11-day moving average. Significant differences, above the 95% confidence level, are displayed by gray shading using the bootstrap analysis with 10,000 times random sampling. The gray dotted lines indicate the zero line.

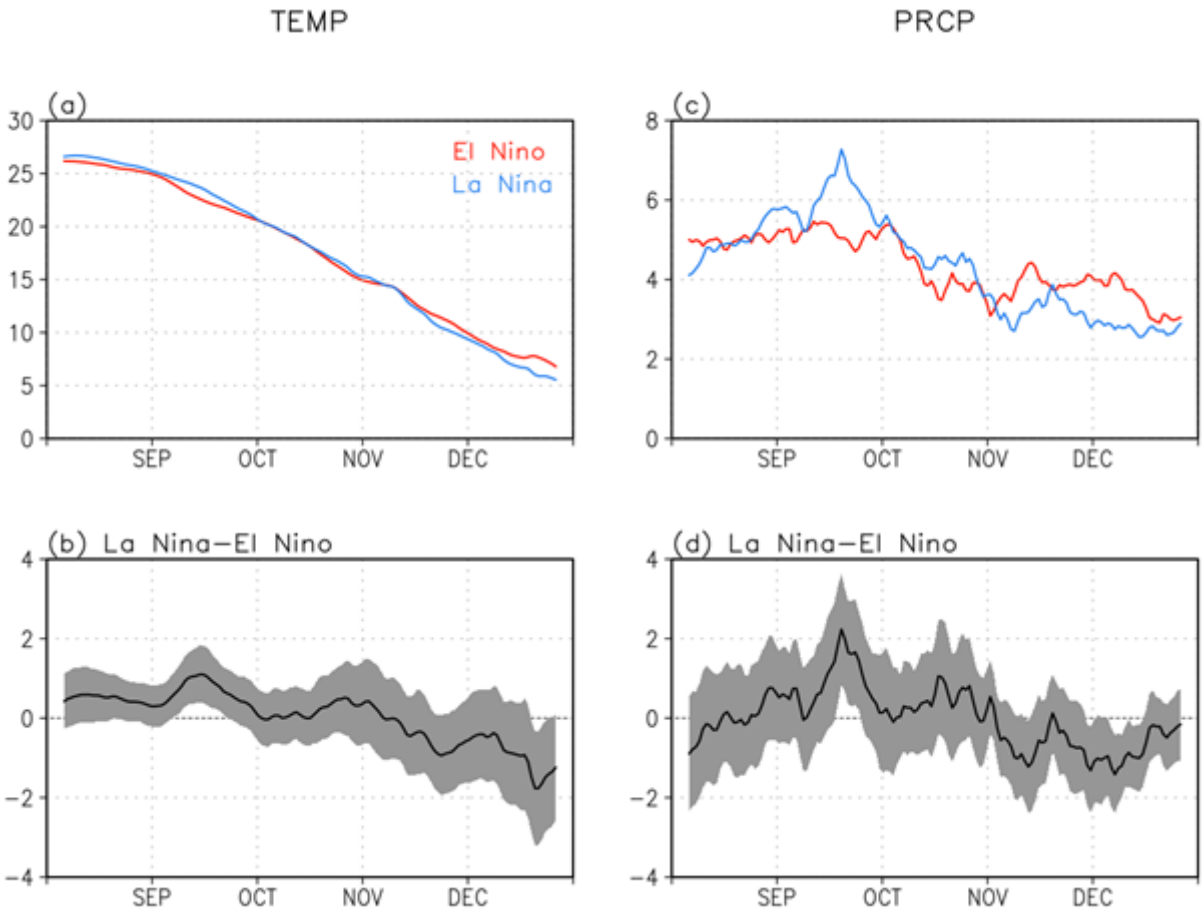

Figure 2

Mean daily (a) air temperature and (c) precipitation from August to December over the Korea-Japan (120°-145°E, 30°-40°N) region for the El Niño (red line; ℃) and La Niña (blue line; mm/day) years based on the ±0.5 standard deviation of SON Niño3.4 (170°-120°W, 5°S-5°N) SST. Difference in the (b) temperature and (d) precipitation between El Niño and La Niña years. Temperature and precipitation data are filtered with an 11-day moving average. Significant differences, above the 95% confidence level, are displayed by gray shading using the bootstrap analysis with 10,000 times random sampling. The gray dotted lines indicate the zero line.

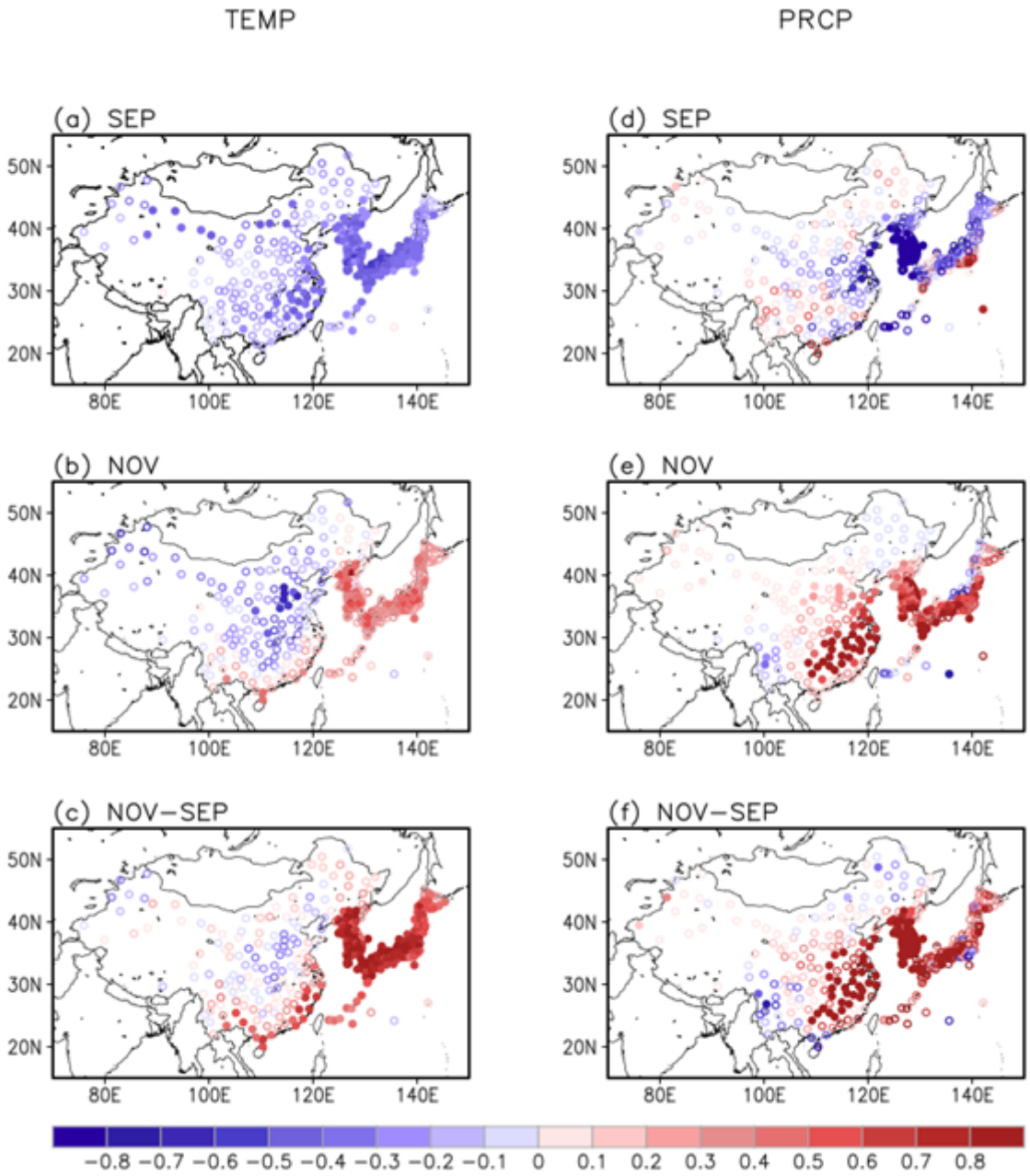

Figure 3

Regression coefficients of temperature (℃; left panels) and precipitation anomalies (mm/day; right panels) corresponding to the SON Niño3.4 (170°-120°W, 5°S-5°N) SST in (a, b) September, (c, d) November, and for (e, f) the difference between September and November. Values over the 95% confidence level based on the student t-test are denoted by closed circles. Note: The designations employed and the presentation of the material on this map do not imply the expression of any opinion whatsoever on the part of Research Square concerning the legal status of any country, territory, city or area or of its authorities, or concerning the delimitation of its frontiers or boundaries. This map has been provided by the authors.

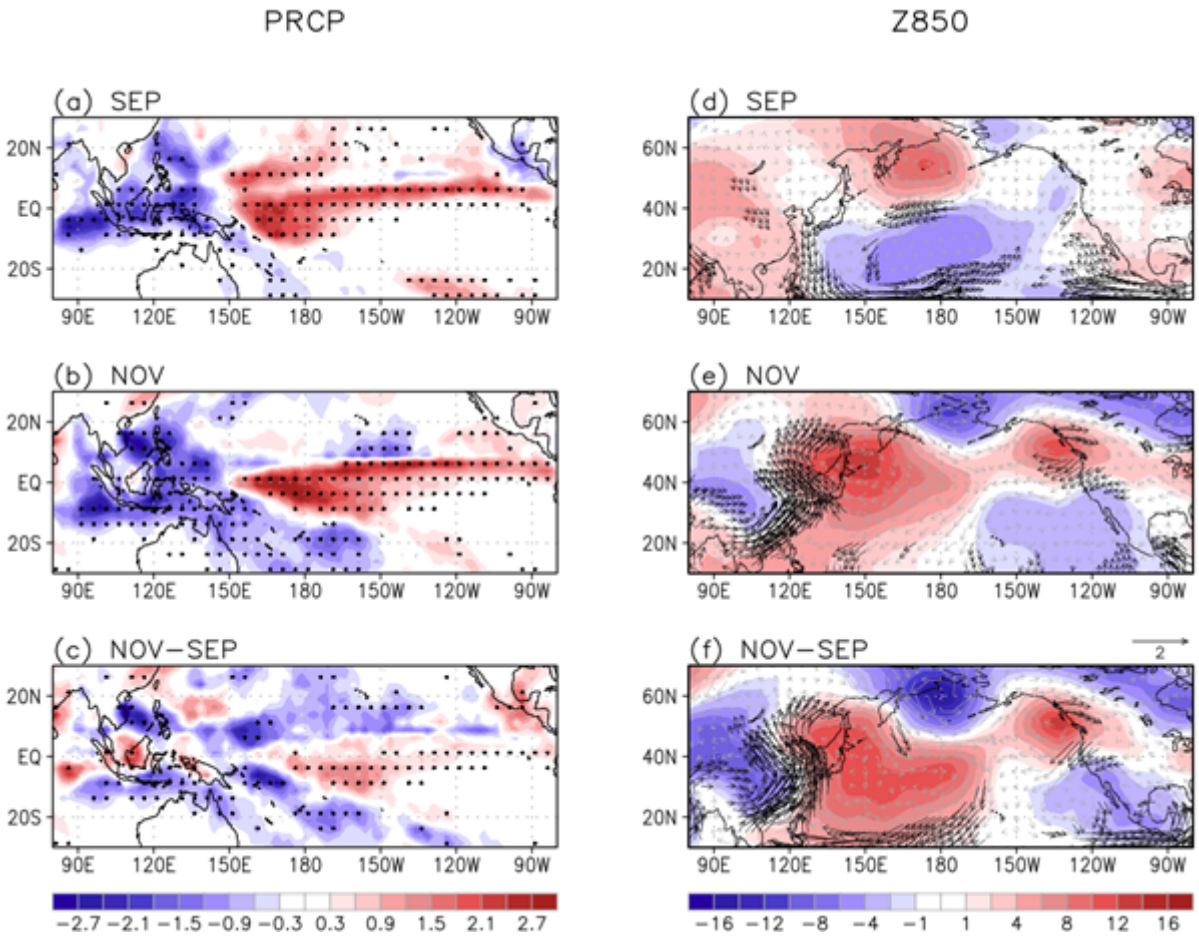

Figure 4

Regression of precipitation (mm/day; left panels) anomalies, 850hPa geopotential height (shading; m; right panels), and wind (vector; m/s) anomalies with respect to the SON Niño3.4 (170°-120°W, 5°S-5°N) SST in (a, b) September, (c, d) November, and for (e, f) the difference between September and November. Regions where the anomalous precipitation is statistically significant, above the 95% confidence level, are stippled (left panels). Values over the 95% confidence level based on the student t-test are denoted by black winds (right panels).

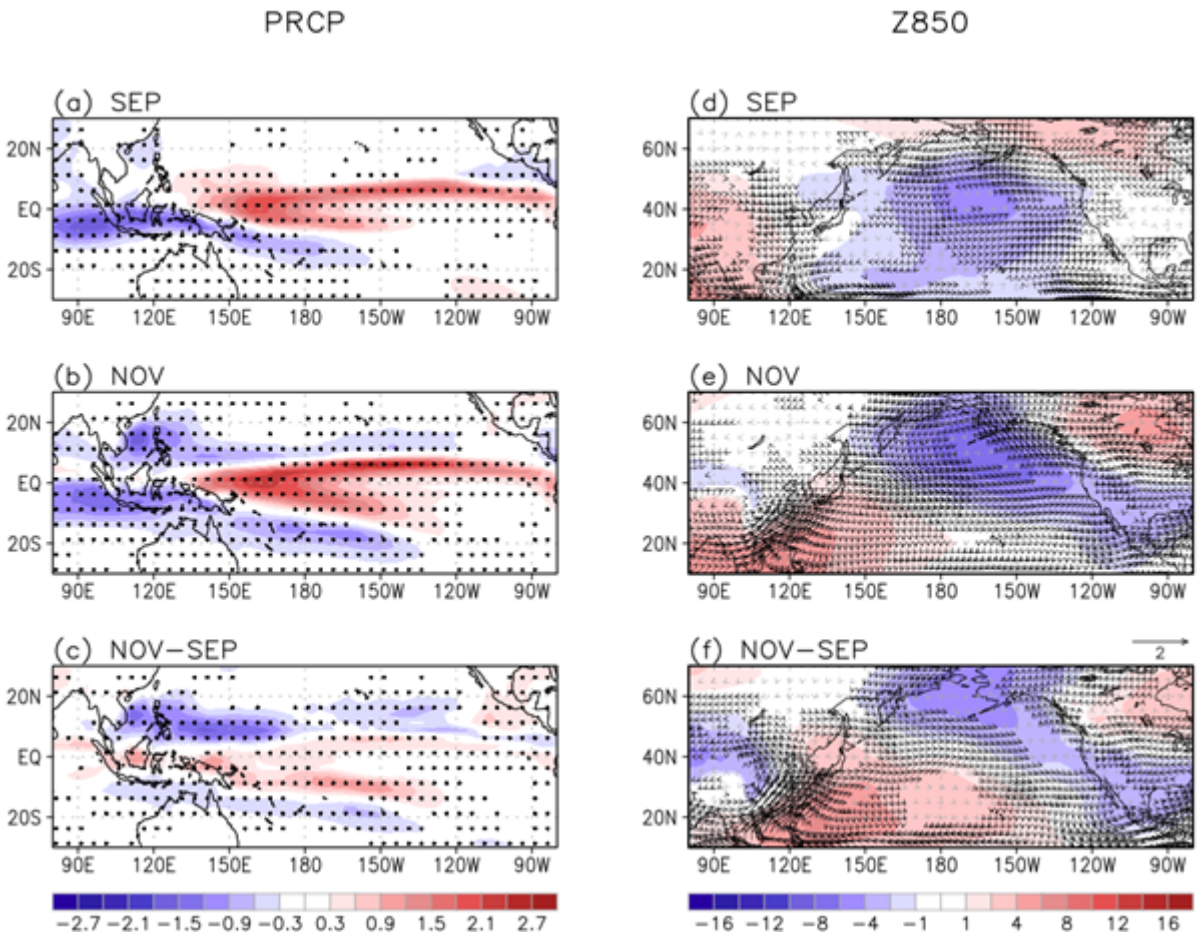

Figure 5

Regression of precipitation (mm/day; left panels) anomalies, 850hPa geopotential height (shading; m; right panels), and wind (vector; m/s) anomalies with respect to the SON Niño3.4 (170°-120°W, 5°S-5°N) SST for the CMIP5 MME in (a, b) September, (c, d) November, and for (e, f) the difference between November and September. Regions where the anomalous precipitation is statistically significant, above the 90% confidence level, are stippled (left panels). Values over the 95% confidence level based on the student t-test are denoted by black winds (right panels).

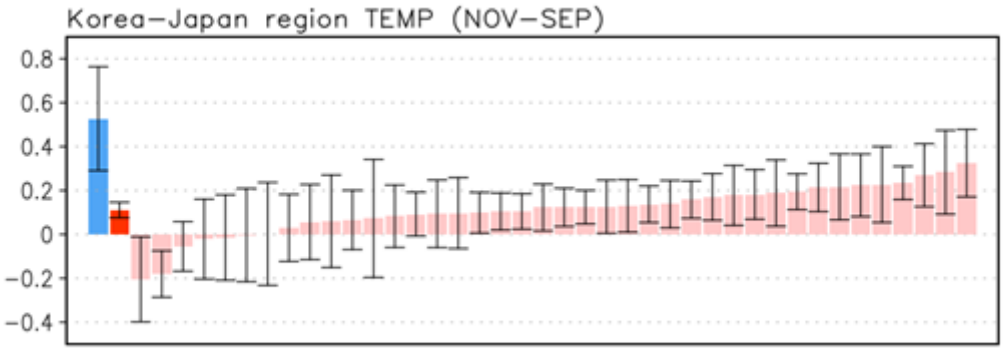

Figure 6

The area-averaged regression differences (November-September) in air temperature over the Korea-Japan region (120°-145°E, 30°-40°N) regressed with respect to SON Niño3.4 (170°-120°W, 5°S-5°N) SST from observations (blue bar), CMIP5 MME (red bar), and individual models (pink bars). Black intervals indicate the 95% confidence level based on the student t-test.

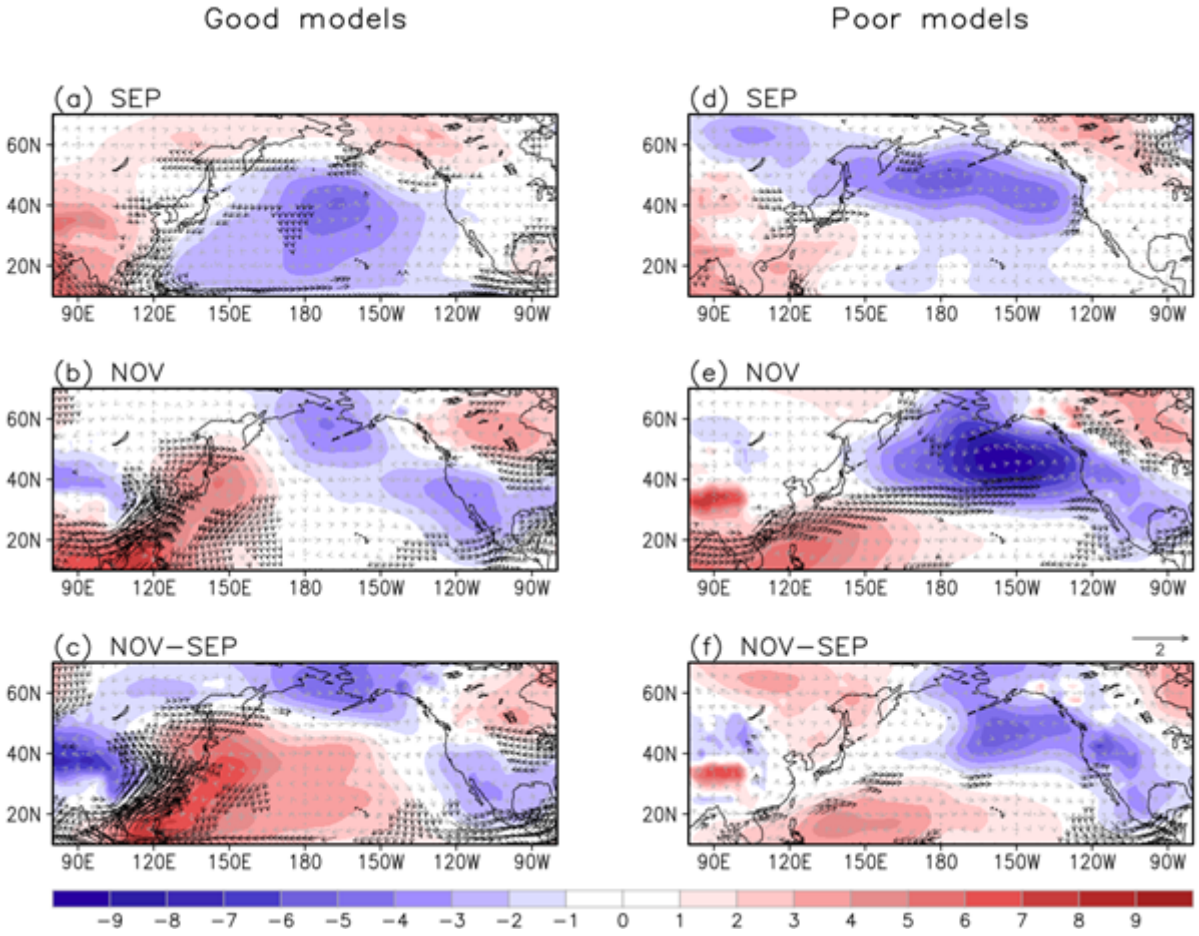

Figure 7

Composites of regressed 850hPa geopotential height (shading; m), and wind (vector; m/s) anomalies for the good (left panels) and poor (right panels) models with respect to the SON Niño3.4 (170°-120°W, 5°S-5°N) SST in (a, b) September, (c, d) November, and for (e, f) the difference between November and September. Values over the 95% confidence level based on the student t-test are denoted by black winds. The good and poor models are classified as the 10 highest and 10 lowest models, respectively, based on the regression values in Fig. 6.

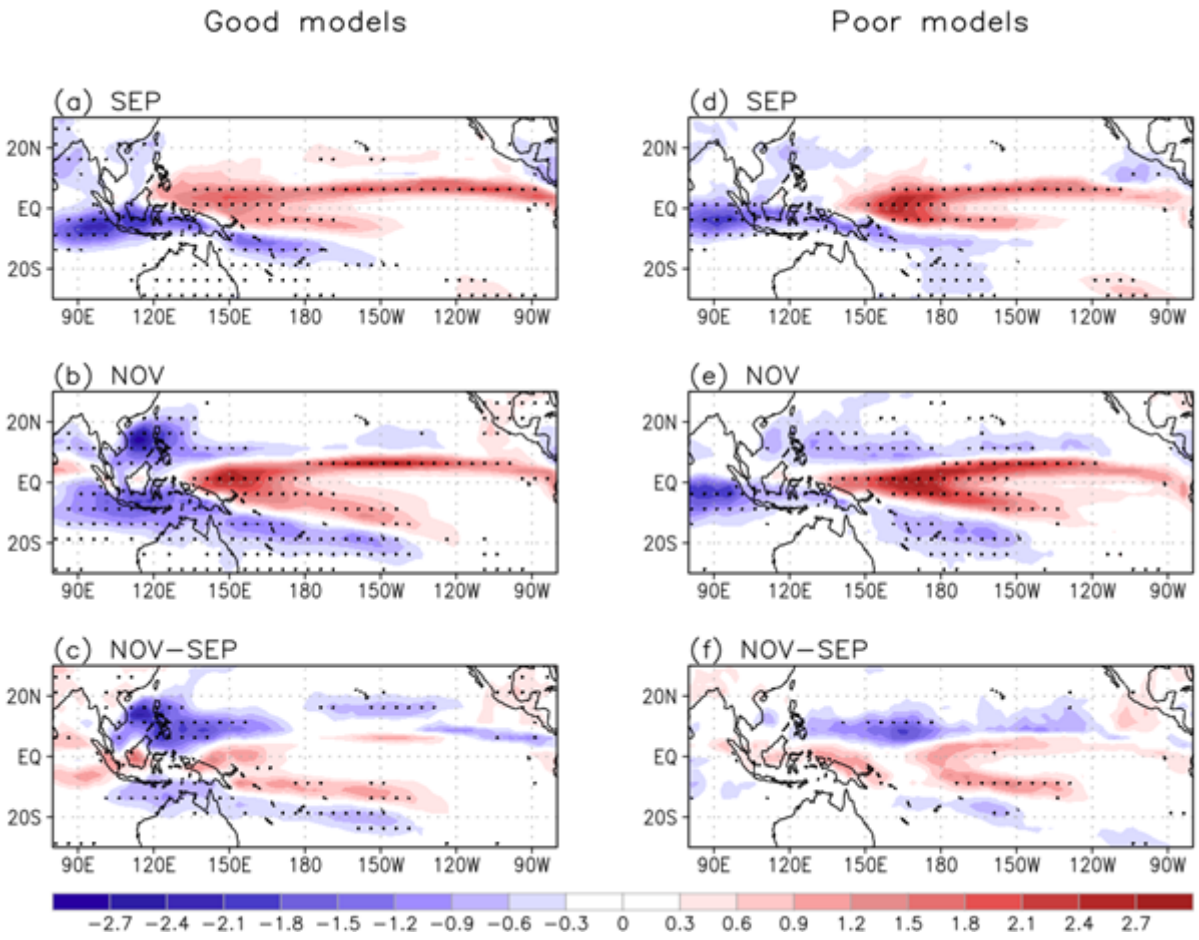

Figure 8

Composites of regressed precipitation (mm/day) anomalies for the good (left panels) and poor (right panels) models with respect to the SON Niño3.4 (170°-120°W, 5°S-5°N) SST in (a, b) September, (c, d) November, and for (e, f) the difference between November and September. Regions where the anomalous precipitation is statistically significant, above the 95% confidence level, are stippled. The good and poor models are classified as the 10 highest and 10 lowest models, respectively, based on the regression values in Fig. 6.